Analytical CPP in rotated energy-mapped stress space applied to von-Mises and Drucker-Prager yield surfaces

Diogo Cecílio

Analytical CPP in rotated energy-mapped stress space applied to von-Mises and Drucker-Prager yield surfaces

Diogo L. Cecílio
Universidade de São Paulo
Brazil

February 21, 2019

Abstract

This study describes a simplified method to formulate the closest point projection (CPP) for associative models. It represents the elastoplastic model on a rotated energy-mapped stress space (REMSS). The CPP in conventional stress space does not give the closest point in Euclidean norm, but in energy norm. In REMSS the correct return trajectory is a closest-point return. REMSS allows to find models that are analytically solvable. The rotated stresses aim in simplifying the constitutive relation allowing to get analytical solutions or applying the Newton's method at a smaller system of equations. The analytical solution is up to four times faster than a standard numerical backward Euler algorithm. The rotated space described here allows to drop one cylindrical coordinate, i.e., instead of using three coordinates (e.g. ξ, ρ and β) to represent a yield surface in principal stress space, at most two are necessary (e.g. ξ and/or β). The analytical CPP solution using the proposed method is described for Druker-Prager and von Mises models. This study also discuss the numerical solution of modified hyperbolic Drucker-Prager. The proposed formulation is verified by applying it to three finite element examples and the code is available on-line. Extent of the code proposed here to elastoplastic calculations of other models is straightforward.

Keywords closest point projection, rotated energy-mapped stress space, computational plasticity, finite elements, Mathematica

1 Introduction

The non-linear Finite Element solution of an elastoplastic analysis is separated in two levels. At the material level, the constitutive equations must be integrated for a given strain increment and a load history for every integration point. At the global equilibrium level, the internal stresses must be balanced with the external loads. The method adopted to integrate the constitutive equations at the material level directly control the accuracy and stability of the finite element solution. There are two main lines adopted to integrate the constitutive equations at the material level: explicit forward Euler and implicit backward Euler.

The explicit methods first appear in [1, 2, 3]. This technique computes the yield function, the flow rule and the hardening law at a known stress, allowing the solution of complex models, but at the same time it does not enforce consistency, making control error algorithms and small load steps necessary.

Implicit Backward Euler integration schemes have achieved much popularity over the past two decades [4, 5, 3, 6, 7, 8]. In implicit methods, stress and hardening variables are unknown, resulting in a non-linear set of equations that must be solved iteratively. The implicit technique to integrate the elastoplastic equations is known as Return Mapping Algorithm (RMA). In this formulation, the numerical integration is divided into two main steps: an elastic trial step and a plastic correction step (or return-mapping algorithm). If the trial stress computed in the first step fails to verify the plastically admissible condition, it is returned to the yield surface using Newton's method to solve the non-linear system of equations. The implicit return mapping can be interpreted as a closest point projection (CPP) of the trial stress onto a returned stress in the yield surface [9, 10, 12, 8].

As pointed by [11], in conventional stress space (SS) the closest point projection (CPP) of computational plasticity in general does not provide the closest point to the trial stress in a Euclidean sense, but rather in energy metrics. The CPP will be provided in a Euclidean sense only when the Poisson coefficient is zero or for the simple case explored by [13], where the author proposed the radial return method, following the von Mises yield criterion with perfect plasticity. Thus, if a trial stress is projected onto the yield surface in the conventional stress space, the project path will be oblique to the yield surface, except in the simple cases discussed above. In this study, inspired by [11] and [14], a new stress space is proposed, in which a yield surface's parametrization and a rotation matrix are introduced to transform the stresses from the conventional stress space (SS) to a rotated energy mapped stress space (REMSS).

In REMSS, the projection direction will be aligned with the plastic flow rule and the distance between the trial and the returned stress will be the closest. Determining the CPP in the REMSS is an intuitive task in which it is possible to graphically identify the smallest distance between two points and calculate it by taking the Euclidean norm of the vector formed by the difference between these two points (e.g. trial and returned stresses). In addition, it makes it possible to verify if the algorithm is working properly by calculating the internal product of the projection direction in relation to the direction parallel to the plastic surface and verifies if they are perpendicular.

A rotation is introduced to simplify the CPP by orienting the stress axes to coincide with the hydrostatic coordinate. This rotation enables rewriting the constitutive matrices in a diagonal form, having as a consequence the RMA simplification. If in case the yield surface does not depend on the Lode angle (e.g., von Mises or Drucker-Prager models), the closest point to the admissibility surface will have the same lode angle. This means the solution can be found by varying only one parameter. For some plasticity surfaces, in case of associative models without hardening, the closest point can be computed analytically. This is the case of the von Mises criterion (projection on a cylinder) or Drucker-Prager (projection on a cone). The analytical solution is up to four times faster than a standard numerical backward Euler algorithm [15]. In this study, the analytical solutions for both models are obtained in closed form. When the estimate of the projected point is sufficiently close to the target point, the distance function is a convex function of the variables which parametrize the surface. Therefore, algorithms used to minimize the distance of a point to a surface are more stable than Newton's method for the resolution of a general non-linear system of equations.

The elastoplastic constitutive model in a Finite Element framework is well-known and widely used for solving computation problems in Engineering and Physics. However, the implementation of a clear step-by-step program in *Wolfram Mathematica* environment has yet to been reported. The finite element code discussed here is available online.

2 Finite Element Formulation

The mechanical problem consists of finding the displacement field $\boldsymbol{u}$ that is the solution of the following problem:

$$\begin{cases} div(\boldsymbol{\sigma}) + \boldsymbol{b} = \boldsymbol{0} & \text{in } \Omega \\ \boldsymbol{u} = \boldsymbol{0} & \text{on } \Gamma_D \\ \boldsymbol{\sigma}.\boldsymbol{n} = \boldsymbol{t} & \text{on } \Gamma_N \end{cases} \tag{1}$$

where Ω is the material domain, Γ_D is the boundary part of Ω in which displacement is zero (null *Dirichlet* boundary condition), Γ_N is the boundary part of Ω in which traction is known (*Neumann* boundary condition), $\boldsymbol{b}$ is the body force, known in Ω, and $\boldsymbol{t}$ is the traction force known in boundary Γ_N.

2.1 Linearised Virtual Work

Considering the infinitesimal strain

$$\boldsymbol{\varepsilon}(\boldsymbol{u}) = \frac{1}{2}\left(\nabla \boldsymbol{u} + \nabla \boldsymbol{u}^T\right), \tag{2}$$

the weak form of the equilibrium equation is obtained by multiplying Equation 1 by trial function $\boldsymbol{v} \in \mathbf{V}$ and integrating it over the domain as described in 3.

$$\int_\Omega -div(\boldsymbol{\sigma})\boldsymbol{v}\, d\omega - \int_\Omega \boldsymbol{b} \cdot \boldsymbol{v}\, d\omega = 0 \tag{3}$$

Space $\mathbf{V}$ is given in 4, were $[H^1(\Omega)]^2$ denotes the vectorial space of functions, which is square integrable.

$$\mathbf{V} = \{\boldsymbol{v} \in [H^1(\Omega)]^2 \text{ so that } \boldsymbol{v} = \mathbf{0} \text{ in } \Gamma_D\}, \tag{4}$$

Using the divergence theorem (integration by parts) in Equation 3, we get 5.

$$G(\boldsymbol{u}, \boldsymbol{v}) = \int_\Omega \boldsymbol{\sigma} : \nabla \boldsymbol{v}\, d\omega - \int_\Omega \boldsymbol{b} \cdot \boldsymbol{v}\, d\omega - \int_{\Gamma_N} \boldsymbol{t} \cdot \boldsymbol{v}\, ds = 0, \;\; \forall \boldsymbol{v} \in \mathbf{V}, \tag{5}$$

To find the solution in elastic problems, one needs to find the displacement field that satisfies the virtual work functional defined in 5. In the elastoplastic case, it is necessary to use the linearised version of the Equation 5, which from [6], is given by Equation 6.

$$\int_\Omega \mathbf{D}^{ep} : \delta\boldsymbol{\varepsilon} : \nabla \boldsymbol{v}\, d\omega = -\int_\Omega (\boldsymbol{\sigma} : \nabla \boldsymbol{v} - \boldsymbol{b} \cdot \boldsymbol{v})\, d\omega - \int_{\Gamma_N} \boldsymbol{t} \cdot \boldsymbol{v}\, ds, \;\; \forall \boldsymbol{v} \in \mathbf{V}, \tag{6}$$

2.2 Matrix Finite Element Formulation

The weak formulation described by Equation 6 can be rewritten in matrix form, which can be implemented and solved in computer systems. Here, a two dimensional (plane stress and plane strain problems) formulation is discussed.

$$\sum_e \int_{\Omega_e} \mathbf{B}^\mathbf{T}\, \mathbf{D}^{ep}\, \mathbf{B}\; dA_e = -\sum_e \int_{\Omega_e} \Psi^\mathbf{T}\, \boldsymbol{b}\; dA_e + \sum_e \int_{\Omega_e} \mathbf{B}^\mathbf{T}\, \boldsymbol{\sigma}\; dA_e - \sum_e \int_{\Gamma_{e,N}} \Psi^\mathbf{T}\, \boldsymbol{t}\; ds_e \tag{7}$$

Where Ψ is a $2 \times 2n$ matrix of shape functions, defined as:

$$\Psi = \begin{bmatrix} \hat{\psi}_1 & 0 & \hat{\psi}_2 & 0 & \dots & \hat{\psi}_n & 0 \\ 0 & \hat{\psi}_1 & 0 & \hat{\psi}_2 & \dots & 0 & \hat{\psi}_n \end{bmatrix} \tag{8}$$

The matrix described in 9, known as strain-displacement matrix $\mathbf{B}$, is a $3 \times 2n$ matrix.

$$\mathbf{B} = \begin{bmatrix} \frac{\partial \hat{\psi}_1}{\partial x} & 0 & \frac{\partial \hat{\psi}_2}{\partial x} & 0 & \dots & \frac{\partial \hat{\psi}_n}{\partial x} & 0 \\ 0 & \frac{\partial \hat{\psi}_1}{\partial y} & 0 & \frac{\partial \hat{\psi}_2}{\partial y} & \dots & 0 & \frac{\partial \hat{\psi}_n}{\partial y} \\ \frac{\partial \hat{\psi}_1}{\partial y} & \frac{\partial \hat{\psi}_1}{\partial x} & \frac{\partial \hat{\psi}_2}{\partial y} & \frac{\partial \hat{\psi}_2}{\partial x} & \dots & \frac{\partial \hat{\psi}_n}{\partial y} & \frac{\partial \hat{\psi}_n}{\partial x} \end{bmatrix} \tag{9}$$

The global stiffness matrix (Equation 10), the internal force vector (Equation 11) and the external force vector (Equation 12) are computed as a sum of the contributions of all the elements composing the FEM mesh.

$$\mathbf{K}_T = \sum_e \int_{\Omega_e} \mathbf{B}^\mathbf{T}\, \mathbf{D}^{ep}\, \mathbf{B}\; dA_e \tag{10}$$

$$\mathbf{f}^{\mathbf{int}} = \sum_e \int_{\Omega_e} \mathbf{B}^{\mathbf{T}}\, \boldsymbol{\sigma}\, dA_e \tag{11}$$

$$\mathbf{f}^{\mathbf{ext}} = \sum_e \int_{\Gamma_{e,N}} \Psi^{\mathbf{T}}\, \boldsymbol{t}\, ds_e + \sum_e \int_{\Omega_e} \Psi^{\mathbf{T}}\, \boldsymbol{b}\, dA_e \tag{12}$$

Finding the nodal displacement vector $\boldsymbol{u}_{n+1}$ satisfies the incremental finite element equilibrium equation described in 13, and $\mathbf{r}$ is the residual vector.

$$\mathbf{r}(\boldsymbol{u}_{n+1}) = \mathbf{f}^{\mathbf{int}}(\boldsymbol{u}_{n+1}) - \mathbf{f}^{\mathbf{ext}} = \mathbf{0} \tag{13}$$

Newton's method consists of solving the linear system of equations for the load step.

$$\mathbf{K}_T\ \delta\boldsymbol{u} = -\mathbf{r} \tag{14}$$

3 Constitutive elastoplastic model

Total deformation tensor $\boldsymbol{\varepsilon}$ can be divided into two parts: $\boldsymbol{\varepsilon} = \boldsymbol{\varepsilon}_e + \boldsymbol{\varepsilon}_p$, an elastic part $\boldsymbol{\varepsilon}_e$ and a plastic part $\boldsymbol{\varepsilon}_p$. Free energy φ is also divided into portions of elastic $\varphi_e(\boldsymbol{\varepsilon} - \boldsymbol{\varepsilon}_p)$ and plastic contributions $\varphi_p(\alpha)$, in which α is the internal damage variable. The law of elasticity establishes tensor $\boldsymbol{\sigma} = \bar{\rho}\frac{\partial\varphi_e}{\partial\boldsymbol{\varepsilon}_e}$, in which $\bar{\rho}$ is the specific mass in the configuration of reference. The plastic portion is not related to the strain state of the material; instead, it is related to the history of irreversible dissipative processes to which the material was submitted based on three fundamental axioms: an yield criterion, a flow rule, and a hardening law.

- **Yield Criterion**. Describes the transition between the elastic and plastic domains using the plasticity function $\Phi = \Phi(\boldsymbol{\sigma}, A)$, where $A = \overline{\rho}\partial\varphi_p/\partial\alpha$ is the thermodynamic hardening force. The plasticity function assumes non-positive values in an elastic basis and null values in a plastic basis.

- **Flow Rule**. Assumes the existence of a plastic potential function $\Psi = \Psi(\boldsymbol{\sigma}, A)$, which specifies how the plastic deformation tensor $\boldsymbol{\varepsilon}_p$ evolves in a plasticity process $\dot{\boldsymbol{\varepsilon}}_p = \dot{\gamma}\boldsymbol{a}$, in which $\boldsymbol{a}(\boldsymbol{\sigma}, A) = \partial\Psi/\partial\boldsymbol{\sigma}$ is the flow direction, and $\gamma(t)$ is a plastic multiplier.

- **Hardening Law**. Specifies the evolution of internal damage variable $\dot{\boldsymbol{\alpha}} = \dot{\gamma}\boldsymbol{h}$, in which $\boldsymbol{h}(\boldsymbol{\sigma}, A) = -\partial\Psi/\partial A$ is the hardening modulus.

In summary, the elastic-plastic constitutive model is formed by the following initial value problem: initial values $\boldsymbol{\varepsilon}_p(t_0)$ and $\boldsymbol{\alpha}(t_0)$ and the history of infinitesimal deformation tensor $\boldsymbol{\varepsilon}(t)$, $t \in [t_0, T]$ are estimated to find the functions that define plastic deformation tensor $\boldsymbol{\varepsilon}_p(t)$, internal damage variable $\boldsymbol{\alpha}(t)$ and plastic multiplier $\dot{\gamma}(t)$ that give constitutive elastoplastic equations

$$\begin{cases} \dot{\boldsymbol{\varepsilon}}_p = \dot{\gamma}\ \boldsymbol{a} \\ \dot{\boldsymbol{\alpha}} = \dot{\gamma}\ \boldsymbol{h} \end{cases} \tag{15}$$

with restrictions $\dot{\gamma}(t) \geq 0$, $\Phi(\sigma(t), A(t)) \leq 0$, $\dot{\gamma}(t)\Phi(\sigma(t), A(t)) = 0$ in each (pseudo) instant $t \in [t_0, T]$.

3.1 Algorithm for solving the incremental elastoplastic constitutive problem

For the integration of elastoplastic non-linear systems, the use of efficient numerical integration methods is required. Using the implicit Euler method at a step of (pseudo) time $[t_n, t_{n+1}]$ of a loading cycle, given the deformation state $\boldsymbol{\varepsilon}_n$ and the corresponding plastic deformation $\boldsymbol{\varepsilon}_{p,n}$ and the internal state variable $\boldsymbol{\alpha}_n$ at t_n, for prescribed incremental strain $\Delta\boldsymbol{\varepsilon}$, then plastic deformation $\boldsymbol{\varepsilon}_{p,n+1}$, the internal variable $\boldsymbol{\alpha}_{n+1}$ and $\Delta\gamma$ at the next step are obtained as a solution of the problem that consists of an incremental non-linear system of equations

$$\begin{aligned}\boldsymbol{\varepsilon}_{e,n+1} &= \boldsymbol{\varepsilon}_{e,n} + \Delta\boldsymbol{\varepsilon} - \Delta\gamma\, \boldsymbol{a}_{n+1}\\ \boldsymbol{\alpha}_{n+1} &= \boldsymbol{\alpha}_n + \Delta\gamma\, \boldsymbol{h}_{n+1}\end{aligned} \tag{16}$$

for unknown $\boldsymbol{\varepsilon}_{e,n+1}$, $\boldsymbol{\alpha}_{n+1}$ and $\Delta\gamma$, subjected to restrictions

$$\Delta\gamma \geq 0, \quad \Phi(\boldsymbol{\sigma}_{n+1}, A) \leq 0, \quad \Delta\gamma\Phi(\boldsymbol{\sigma}_{n+1}, A) = 0. \tag{17}$$

As shown in [6], the imposition of restrictions suggests a procedure for solving the problem in two major steps. It begins with a purely elastic predictor process (*elastic trial step*), with $\Delta\gamma = 0$. In this case, trial elastic strain $\boldsymbol{\varepsilon}_{e,trial} = \boldsymbol{\varepsilon}_{e,n} + \Delta\boldsymbol{\varepsilon}$ and internal variables $\boldsymbol{\alpha}^t = \boldsymbol{\alpha}_n$ are defined. Then $\boldsymbol{\sigma}^t$ is calculated according to $\boldsymbol{\varepsilon}_e^t$, and the corresponding $\Phi(\boldsymbol{\sigma}^t, A)$ is given. If $\Phi(\boldsymbol{\sigma}^t, A) \leq 0$, a valid solution to the system is reached, and the variables are replaced by the trial ones. Otherwise, a *plastic corrector step* or RMA is performed by reformulating the incremental problem searching $\boldsymbol{\varepsilon}_{e,n+1}$, $\boldsymbol{\alpha}_{n+1}$ and by having $\Delta\gamma$ satisfy

$$\boldsymbol{\varepsilon}_{e,n+1} = \boldsymbol{\varepsilon}_e^t - \Delta\gamma\, \boldsymbol{a}(\boldsymbol{\sigma}_{n+1}, A) \tag{18}$$

$$\boldsymbol{\alpha}_{n+1} = \boldsymbol{\alpha}^t + \Delta\gamma \boldsymbol{h}\, (\boldsymbol{\sigma}_{n+1}, A) \tag{19}$$

$$\Delta\gamma > 0, \qquad \Phi(\boldsymbol{\sigma}_{n+1}, A) = 0 \tag{20}$$

Next, the plastic strain is updated

$$\boldsymbol{\varepsilon}_{p,n+1} = \boldsymbol{\varepsilon}_{p,n} + \Delta\boldsymbol{\varepsilon} - \Delta\boldsymbol{\varepsilon}_e.$$

Where superscript t means trial.

4 Rotated stress space

Instead of using the six stress-independent components for the geometric representation of a state of stress at a given point, a simplified alternative is to adopt principal stresses $\sigma = [\sigma_1, \sigma_2, \sigma_3]^T$ as coordinates. This space, known as Haigh–Westergaard stress space, will be refereed to simply as stress space (SS). The stress tensor is represented in terms of the principal stresses sorted in descending order $\sigma_1 \geq \sigma_2 \geq \sigma_3$, and are calculated by

$$\sigma = \begin{bmatrix} \xi/\sqrt{3} + \sqrt{2/3}\rho\cos(\beta) \\ \xi/\sqrt{3} + \sqrt{2/3}\rho\cos(\beta - 2\pi/3) \\ \xi/\sqrt{3} + \sqrt{2/3}\rho\cos(\beta + 2\pi/3) \end{bmatrix}. \tag{21}$$

Principal stresses are a parametrisation of Haigh–Westergaard cylindrical coordinates ξ, ρ and β ,

$$\xi = \frac{I_1}{\sqrt{3}}, \quad \rho = \sqrt{2J_2}, \quad \beta = \frac{1}{3}\cos^{-1}\left(\frac{3\sqrt{2}}{2}\frac{J_3}{J_2^{3/2}}\right). \tag{22}$$

Constitutive laws can be simplified with the introduction of a new coordinate system of rotated principal variables, similar to the decompositions defined in [16, 17], called a rotated stress space (RSS). The RSS is defined as $\tilde{\sigma} = [\tilde{\sigma_1}, \tilde{\sigma_2}, \tilde{\sigma_3}]^T$, and is defined by

$$\tilde{\sigma} = \begin{bmatrix} \xi \\ \rho\cos(\beta) \\ \rho\sin(\beta) \end{bmatrix}. \tag{23}$$

The RSS can also be computed by the rotation $\boldsymbol{R}$,

$$\boldsymbol{R} = \begin{bmatrix} \frac{1}{\sqrt{3}} & \frac{1}{\sqrt{3}} & \frac{1}{\sqrt{3}} \\ \sqrt{\frac{2}{3}} & -\frac{1}{\sqrt{6}} & -\frac{1}{\sqrt{6}} \\ 0 & \frac{1}{\sqrt{2}} & -\frac{1}{\sqrt{2}} \end{bmatrix}. \tag{24}$$

This transformation relates the principal stresses in SS and RSS, This relation is defined in Equation (25).

$$\tilde{\sigma} = \boldsymbol{R}\, \sigma, \tag{25}$$

in RSS the expressions for the cylindrical coordinates and invariants become simpler,

$$\xi = \tilde{\sigma}_1, \quad \rho = \sqrt{\tilde{\sigma}_2^2 + \tilde{\sigma}_3^2}, \quad \beta = \arctan\left(\tilde{\sigma}_3 / \tilde{\sigma}_2\right). \tag{26}$$

5 CPP in the SS and RSS spaces

The elastic stress-strain relation in SS and RSS are given by

$$\sigma = \mathbf{D}_{ss}\, \varepsilon, \quad \tilde{\sigma} = \mathbf{D}_{rss}\, \tilde{\varepsilon}. \tag{27}$$

Were the elastic constitutive matrices in SS and RSS are given by

$$\mathbf{D}_{ss} = \begin{bmatrix} \left(K + \frac{4G}{3}\right) & \left(K - \frac{2G}{3}\right) & \left(K - \frac{2G}{3}\right) \\ \left(K - \frac{2G}{3}\right) & \left(K + \frac{4G}{3}\right) & \left(K - \frac{2G}{3}\right) \\ \left(K - \frac{2G}{3}\right) & \left(K - \frac{2G}{3}\right) & \left(K + \frac{4G}{3}\right) \end{bmatrix} \tag{28}$$

and

$$\mathbf{D}_{rss} = \boldsymbol{R}^T\, \mathbf{D}_{ss}\, \boldsymbol{R} = \begin{bmatrix} 3K & 0 & 0 \\ 0 & 2G & 0 \\ 0 & 0 & 2G \end{bmatrix}, \tag{29}$$

respectively. Elastic constants K and G are the Bulk and the Shear Modulus, respectively.

Distance equations in SS and RSS are defined as the euclidean norm of the difference between trial and returned stresses in an energy metrics, and are described by Eqs. (30) and (31). Superscripts t and r denote the trial and return stresses.

$$d(\sigma^t, \sigma^r) = \sqrt{(\sigma^t - \sigma^r)^T\, \mathbf{D}_{ss}^{-1}\, (\sigma^t - \sigma^r)} \tag{30}$$

$$d(\tilde{\sigma}^t, \tilde{\sigma}^r) = \sqrt{(\tilde{\sigma}^t - \tilde{\sigma}^r)^T\, \mathbf{D}_{rss}^{-1}\, (\tilde{\sigma}^t - \tilde{\sigma}^r)} \tag{31}$$

The CPP solution consists in minimizing these distances by making their derivatives equal to zero and solving for the state variables (e. g. $\partial d(\sigma^t, \sigma^r)^2 / \partial \sigma^r = 0$ or $\partial d(\tilde{\sigma}^t, \tilde{\sigma}^r)^2 / \partial \tilde{\sigma}^r = 0$).

It is important to note that matrix $\mathbf{D}_{rss}$ is a 3x3 diagonal matrix and implies in significant simplifications in the CPP's formulation:

- For perfect plasticity, the solution to β is analytical and is the same for Drucker-Prager, von Mises and any other model that has circular shape in the deviatoric section.
- Equations are much simpler due to the rotation employed to simplify the constitutive relations.
- For some plasticity surfaces, in case of associative models without hardening, the closest point can be computed analytically. This is the case of the von Mises criterion (projection on a cylinder) or Drucker-Prager criterion (projection on a cone). In this paper, the analytical solution for both models are obtained in closed form.
- When the estimate of the projected point is sufficiently close to the target point, the distance function is a convex function of the variables that parametrize the surface. Therefore, algorithms oriented to minimizing the distance of a point to a surface are more stable than Newton's method for the resolution of a general non-linear system of equations.

6 CPP in EMSS and REMSS

As discussed previously, the CPP consists in minimizing the distance between the trial and returned stress in energy metric in the SS and RSS spaces. Of an Euclidean point of view, this will only be the closest point in a principal stress space for the special case where $2G = 3K$, or for certain simple models such as the von Mises yield criterion.

A new energy-mapped stress space (EMSS) was introduced by [11] and was defined to be equivalent in the Euclidean norm to the conventional stress in the energy norm. In this space, the correct return trajectory is the closest-point return.

The stress vector in EMSS is represented by $\hat{\sigma} = [\hat{\sigma}_1, \hat{\sigma}_2, \hat{\sigma}_3]^T$, and can be computed by

$$\hat{\sigma} = \hat{\boldsymbol{T}}\sigma, \tag{32}$$

were

$$\hat{\boldsymbol{T}} = \begin{bmatrix} \frac{1}{9}(3\sqrt{2}\sqrt{\frac{E}{G}} + \sqrt{3}\sqrt{\frac{E}{K}}) & \frac{1}{18}(-3\sqrt{2}\sqrt{\frac{E}{G}} + 2\sqrt{3}\sqrt{\frac{E}{K}}) & \frac{1}{18}(-3\sqrt{2}\sqrt{\frac{E}{G}} + 2\sqrt{3}\sqrt{\frac{E}{K}}) \\ \frac{1}{18}(-3\sqrt{2}\sqrt{\frac{E}{G}} + 2\sqrt{3}\sqrt{\frac{E}{K}}) & \frac{1}{9}(3\sqrt{2}\sqrt{\frac{E}{G}} + \sqrt{3}\sqrt{\frac{E}{K}}) & \frac{1}{18}(-3\sqrt{2}\sqrt{\frac{E}{G}} + 2\sqrt{3}\sqrt{\frac{E}{K}}) \\ \frac{1}{18}(-3\sqrt{2}\sqrt{\frac{E}{G}} + 2\sqrt{3}\sqrt{\frac{E}{K}}) & \frac{1}{18}(-3\sqrt{2}\sqrt{\frac{E}{G}} + 2\sqrt{3}\sqrt{\frac{E}{K}}) & \frac{1}{9}(3\sqrt{2}\sqrt{\frac{E}{G}} + \sqrt{3}\sqrt{\frac{E}{K}}) \end{bmatrix}. \tag{33}$$

A rotated energy mapped stress space (REMSS) has it's coordinates $\bar{\sigma} = [\bar{\sigma_1}, \bar{\sigma_2}, \bar{\sigma_3}]^T$, and is given by

$$\bar{\sigma} = \bar{\boldsymbol{T}}\,\tilde{\sigma}, \tag{34}$$

with

$$\bar{\boldsymbol{T}} = \boldsymbol{R}^T\,\hat{\boldsymbol{T}}\,\boldsymbol{R} = \begin{bmatrix} \sqrt{\frac{E}{3K}} & 0 & 0 \\ 0 & \sqrt{\frac{E}{2G}} & 0 \\ 0 & 0 & \sqrt{\frac{E}{2G}} \end{bmatrix}. \tag{35}$$

The distance equation in EMSS and in REMSS are described by

$$d(\hat{\sigma}^t, \hat{\sigma}^r) = \sqrt{\frac{1}{E}\,(\hat{\sigma}^t - \hat{\sigma}^r)^T\,(\hat{\sigma}^t - \hat{\sigma}^r)}, \tag{36}$$

and

$$d(\bar{\sigma}^t, \bar{\sigma}^r) = \sqrt{\frac{1}{E}\,(\bar{\sigma}^t - \bar{\sigma}^r)^T\,(\bar{\sigma}^t - \bar{\sigma}^r)}. \tag{37}$$

To obtain the full stress tensor $\boldsymbol{\sigma}$, first the returned cylindrical variables (i.e. ξ^r, ρ^r and β^r) have to be substituted in Eq. (21) to get the principal returned stress σ_i^r, and the

$$\boldsymbol{\sigma} = \sum_{i=1}^{3} \sigma_i^r\,(e_i \otimes e_i). \tag{38}$$

7 Solution examples in REMSS

The closest point projection in REMSS is equivalent to minimizing the distance in this space. The distance function in REMSS can be computed by using the Euclidean norm of the projection's stress vector, which is computed as the difference of two points: trial stresse $\bar{\sigma}^t$ and retuned stress $\bar{\sigma}^r$ in REMSS. Next, the CPP's closed solution for von Mises and Drucker-Prager models will be discussed, and also a numerical solution to modified Drucker-Prager.

7.1 von Mises

The von Mises yield surface is a cylinder in the stress space. The surface, considering a perfectly plastic model, is given by

$$\Phi = \sqrt{3/2}\rho - \sigma_y, \tag{39}$$

were σ_y is the material yield stress in uniaxial tension. The cylinder radius is constant and can be computed by making Equation (39) equal to zero. The result is given by Equation (40), which is the radial returned deviatoric coordinate. Equation (40) also gives the return hydrostatic coordinate, which is equal to the trial one

$$\rho^r = \sigma_y\sqrt{2/3}\ , \xi^r = \xi^t. \tag{40}$$

The returned stresses in yield surface $\bar{\sigma}^r$ can be computed by substituting Equation (40) in (23) and then in (34), to get

$$\bar{\sigma}^r = \frac{1}{\sqrt{3}} \begin{bmatrix} \xi^r\sqrt{\frac{E}{K}} \\ \sigma_y\sqrt{\frac{E}{G}}\cos(\beta^r) \\ \sigma_y\sqrt{\frac{E}{G}}\sin(\beta^r) \end{bmatrix}, \tag{41}$$

were the only unknown is β^r. The trial stress in REMSS is computed by

$$\bar{\sigma}^t = \bar{T}\boldsymbol{R}\sigma^t. \tag{42}$$

Substituting Equations (42) and (41) in (37) results in the distance function

$$\begin{aligned} d(\bar{\sigma}^t, \bar{\sigma}^r)^2 = \frac{4\left(\sigma_1^t + \sigma_2^t + \sigma_3^t - \sqrt{3}\xi^r\right)^2}{36K} + \frac{3\left(-2\sigma_1^t + \sigma_2^t + \sigma_3^t + 2\sigma_y\cos(\beta^r)\right)^2}{36G} + \\ \frac{\left(-3\sigma_2^t + 3\sigma_3^t + 2\sqrt{3}\sigma_y\sin(\beta^r)\right)^2}{36G}, \end{aligned} \tag{43}$$

to be minimized with respect to β^r. Deriving Equation (43) in relation to β, equaling it to zero and then solving it to obtain the β provides the analytical solution (44). To obtain the projected or returned principal stresses, it is necessary to substitute Equations (44) and (40) in (21).

$$\beta^r = -\arctan\left(\frac{\sqrt{3}(\sigma_2^t - \sigma_3^t)}{-2\sigma_1^t + \sigma_2^t + \sigma_3^t}\right). \tag{44}$$

As previously discussed in [13], in the von Mises model the CPP will be perpendicular to the yield surface in all stress spaces mentioned above, even with $\nu \neq 0$. Figure 1 illustrates this fact, showing the projection vector is perpendicular to the yield surface in all spaces.

7.2 Drucker-Prager

The Drucker-Prager yield surface is a cone in the stress space. The surface considering a perfectly plastic model is given by

$$\Phi = \frac{\rho}{\sqrt{2}} + A\frac{\sqrt{3}\xi}{3} - Bc, \tag{45}$$

were c is the material cohesion, A and B are constants that depend on the internal friction angle ϕ. For plane strain match [6], the constants are given by

$$A = 3\tan(\phi)/\sqrt{9 + 12\tan(\phi)^2},\ \ B = 3/\sqrt{9 + 12\tan(\phi)^2}. \tag{46}$$

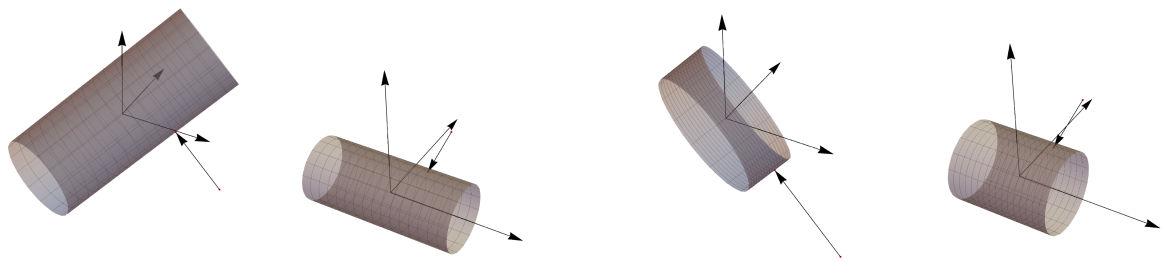

(a) (b) (c) (d)

Figure 1: CPP in the von Mises yield surface. The figures show the projections in the following spaces a) SS, b) RSS, c) EMSS and d) REMSS. To generate the surfaces, the following values for the constants were adopted: $E = 210000MPa$, $\nu = 0.3$ and $\sigma_y = 210MPa$.

The cone radius depends on the hydrostatic component ξ^r and can be computed by making Equation (45) equal to zero and solving for ρ^r,

$$\rho^r = \sqrt{2}\, B\, c - \sqrt{\frac{2}{3}}\, A\, \xi^r, \tag{47}$$

which is the radial returned deviatoric coordinate.

The returned stresses on yield surface $\bar{\sigma}^r$ is computed by substituting (47) in Equation (23) and then in Equation (34) to get

$$\bar{\sigma}^r = \begin{bmatrix} \frac{\xi^r \sqrt{\frac{E}{K}}}{\sqrt{3}} \\ \frac{1}{3}\left(3Bc - \sqrt{3}A\xi^r\sqrt{\frac{E}{G}}\cos(\beta^r)\right) \\ \frac{1}{3}\left(3Bc - \sqrt{3}A\xi^r\sqrt{\frac{E}{G}}\cos(\beta^r)\right) \end{bmatrix}. \tag{48}$$

Substituting (42) and (48) in (37) to get the distance function

$$\begin{gathered} d(\bar{\sigma}^t, \bar{\sigma}^r)^2 = \frac{4\left(\sigma_1^t + \sigma_2^t + \sigma_3^t - \sqrt{3}\xi^r\right)^2}{36K} + \\ \frac{\left[\sqrt{3}\left(2\sigma_1^t - \sigma_2^t - \sigma_3^t\right) + \left(-6Bc + 2\sqrt{3}A\xi^r\right)\cos(\beta^r)\right]^2}{36G} + \\ \frac{\left[3\left(\sigma_2^t - \sigma_3^t\right) + \left(-6Bc + 2\sqrt{3}A\xi^r\right)\sin(\beta^r)\right]^2}{36G} \end{gathered} \tag{49}$$

to be minimized in terms of ξ and β. Here β^r has the same analytical solution obtained above to von Mises model.

The minimum is found deriving Equation (49) in relation to ξ^r, equaling to zero and solving for ξ^r, to get

$$\xi^r = \frac{-3AK\left(2\sigma_1^t - \sigma_2^t - \sigma_3^t\right)\cos(\beta^r) + \sqrt{3}\left[6ABcK + 2G\left(\sigma_1^t + \sigma_2^t + \sigma_3^t\right) - 3AK\left(\sigma_2^t - \sigma_3^t\right)\sin(\beta^r)\right]}{6\left(G + A^2K\right)}. \tag{50}$$

To change the Mohr-Coulomb's fit (e.g. inner, outer match), the constants A and B (here defined to be plane strain match) have to be changed.

Returned principal stresses are obtained by the substitution of the Equations (50), (47) and (44) in (21). Figure 2 illustrates the discussion above, showing that the CPP method is not the perpendicular to the yield surface in spaces SS and RSS, but it is in spaces EMSS and REMSS. To generate surfaces of Figure 2, the constants detailed in Table (2) were used.

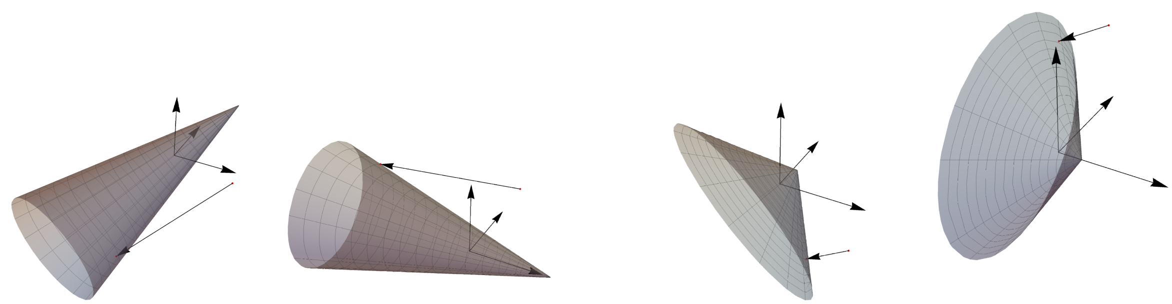

(a) (b) (c) (d)

Figure 2: CPP in the Drucker-Prager yield surface. The figures show the projections in the following spaces: a) SS, b) RSS, c) EMSS and d) REMSS

7.3 Modified Drucker-Prager

A Modified Drucker-Prager yield surface were the hydrostatic tensile apex is removed through the use of hyperbolic meridians, as illustrated in Figure (3). The modified Drucker-Prager with perfectly plasticity is given by

$$\Phi = \left(\frac{c\cot(\phi) - \xi/\sqrt{3}}{A_{md}}\right)^2 - \left(\frac{\rho/\sqrt{2}}{B_{md}}\right)^2 - 1, \tag{51}$$

were c is the material cohesion, A_{md} and B_{md} are constants that depend on internal friction angle ϕ. Constants A_{md} and B_{md} are chosen to be equivalent to Mohr-Coulomb plane strain match, and are detailed in Eq. (59).

The radial returned deviatoric coordinate ρ^r depends on the hydrostatic component ξ^r and is computed by making Equation (51) equal to zero,

$$\rho^r = \sqrt{-\frac{2B_{md}^2\left(3A_{md}^2 - 3\left(c\cot(\phi)\right)^2 + 2\sqrt{3}\,c\cot(\phi)\xi^r - (\xi^r)^2\right)}{3A_{md}^2}}. \tag{52}$$

The returned stresses and the distance function can be obtained using analogous process as discussed for the models above. An important observation is that here β^r is also computed analytically using Eq. (44). Thus the solution of this model is reduced to minimizing the distance function (quartic equation) for only one variable: ξ^r. Analytical solution to this model can be found using the symbolic package *Mathematica*. Although analytical solution exists for this model, it is too cumbersome, and for this reason is not shown here. For simplicity, in this study, the Newton's method is employed to minimize the distance function in REMSS.

Several trial stresses were randomly generated and projected on the yield surface of the modified Drucker-Prager in REMSS. As the stresses are oriented in descending order, only one part of the yield surface is active, as illustrates Figure (4). Due to the high non-linearity of the apex, some convergence difficulties were faced

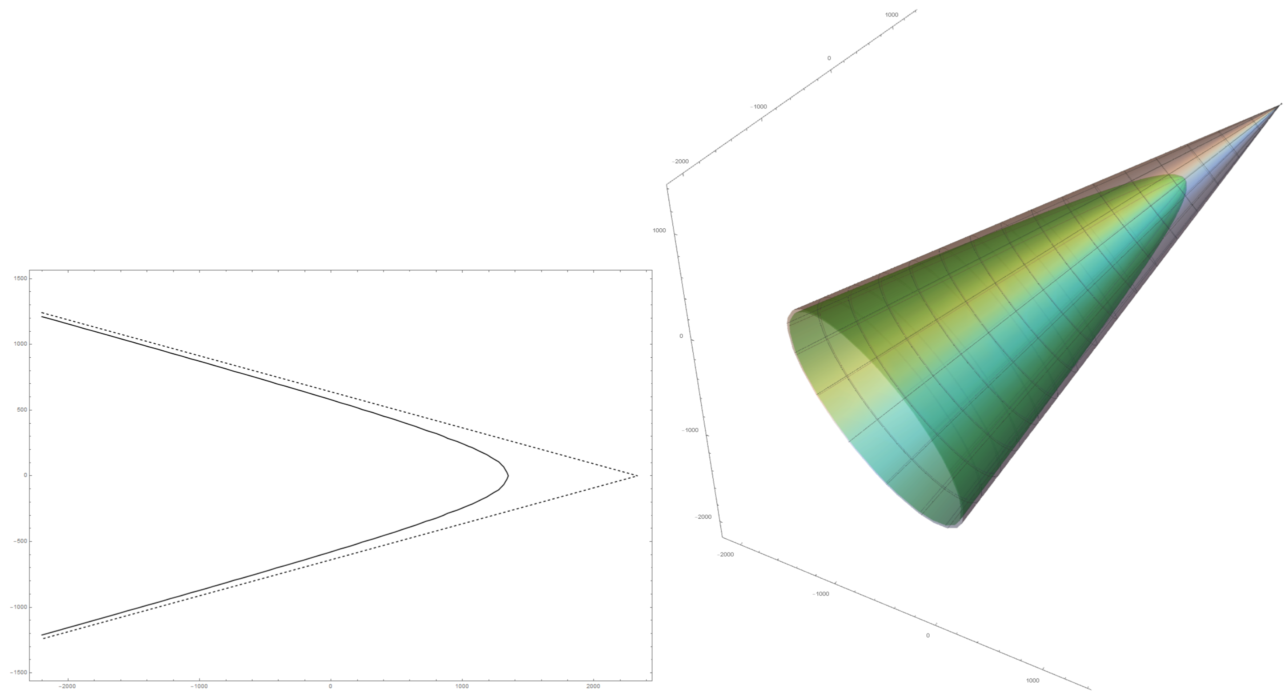

(a) (b)

Figure 3: Drucker-Prager yield surface in: (a) hydrostatic, versus deviatoric, stress space and (b) principal stress space showing both the hyperbolic and original cones.

when using the build in *NMinimize*[1] method of *Mathematica*. The problem was solved by using a "good" initial guess to feed the algorithm.

8 Examples

As an application of the discussed formulation, three numerical examples are considered in this section. In the first example, a long metallic thick-walled cylinder subjected to internal pressure is simulated. The obtained solutions are verified with the analytical solution available in literature. In the second example, the application of the finite element method for the determination of the bearing capacity (limit load) of a strip footing is considered. Also, in this example, a comparison between the modified and common Drucker-Prager is discussed. In example three, the finite element simulation of an inclined earth embankment subjected to self-weight is performed. The solution obtained with hyperbolic Drucker-Prager is compared with Mohr-Coulomb. The cylindrical arc-length method was used to enable the solution algorithms to pass the problems limit load points.

The code written in *Mathematica* is available to download in `https://github.com/diogocecilio/FEM-plasticity`.[2]

8.1 Example 1

In this example, the behavior of a long steel thick-walled cylinder subjected to a prescribed internal pressure P in the inner surface is simulated, considering the von Mises perfectly plastic model. The elastic constants of the

[1]*NMinimize* is a function to find the global minimum of a equation.

[2]The code was written in the *Wolfram Mathematica* 11.0.1.0 version.

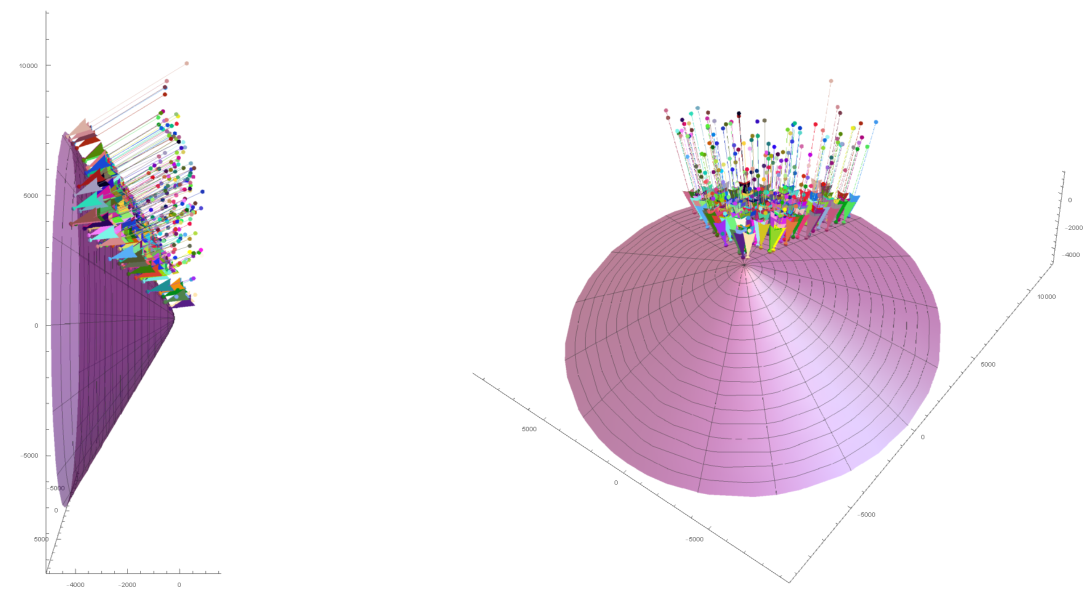

(a) (b)

Figure 4: CPP in the Modified Drucker-Prager yield surface. The figures show the projections in REMSS. Random trial stresses are projected on the yield surface.

material are $E = 210GPa$, $\nu = 0.3$ and $\sigma_y = 0.24GPa$. The cylinder has $100mm$ and $200mm$ internal and external radius, respectively. The mesh, illustrated in Figure 5, is composed by twelve nine-noded elements. The plane strain condition is assumed. Due to the symmetry, only a quarter of the cylinder cross-section is discretized. Null displacements are imposed in the horizontal and vertical direction on the left and bottom edge, respectively. Pressure P is gradually increased until it reaches the limit burst pressure. Fifteen load steps are applied.

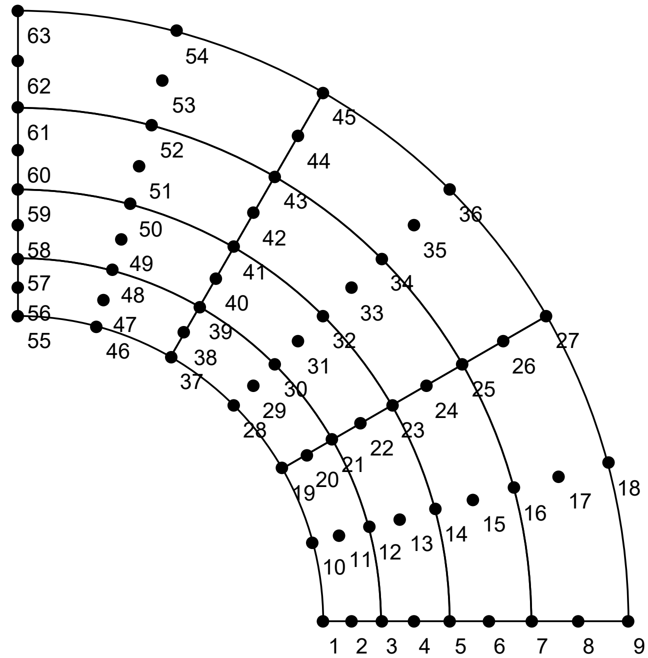

Figure 5: Internally pressurized cylinder. Geometry and finite element mesh.

Figure 6 shows the node's nine radial displacement versus the applied pressure. The solid line is the analytical solution provided by [18] and the points are the FEM solution. The numerical solution proves to be an excellent approximation of the analytical one. Note that the arc-length method allows the numerical simulation to continue, even after the limit load is reached.

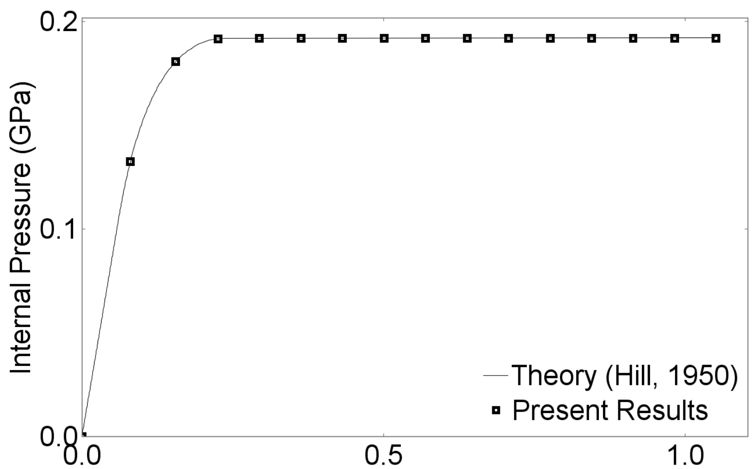

Figure 6: Internally pressurized cylinder. Pressure versus displacement diagram.

Figure 7 shows that the plastic yielding starts at the inner surface and develops gradually toward the outer face of the cylinder. Rupture occurs when the plastic face reaches the outer face and the entire cylinder becomes plastified. At the limit load, the cylinder can expand indefinitely without further increase in the applied pressure. A closed-form solution to this problem has been derived by [18].

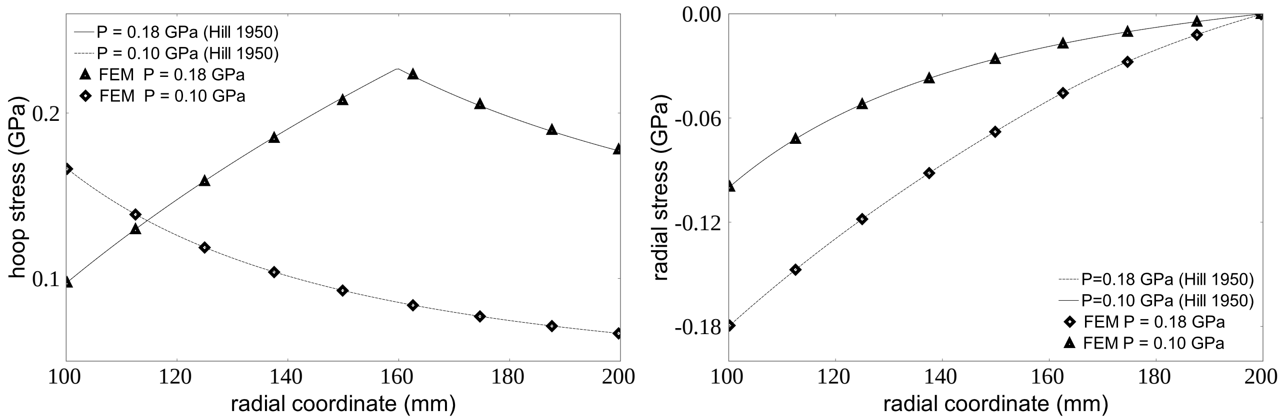

(a) (b)

Figure 7: Hoop (7a) and radial (7b) stress distributions at different applied internal pressures. The finite element results are computed at the Gauss integration points.

8.2 Example 2

In this example, a finite element analysis of the plastic limit load of strip foundations is considered. The solution of associative Modified and common Drucker-Prager models are compared. The constants A, B, A_{md} and B_{md} are defined to be the Drucker–Prager approximation to the Mohr–Coulomb law in plane strain match. The problem material data is described in Table (1). Plane strain analysis is adopted. The soil is assumed to be weightless. The mesh has a total of 240 eight-noded quadrilaterals elements.

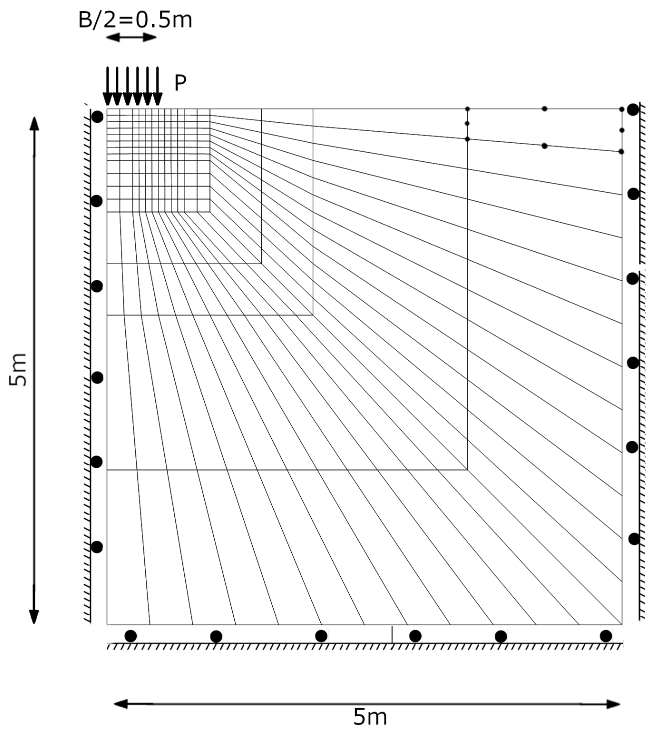

Figure 8: Strip footing mesh.

The loading consists of the increasing value of the pressure P. The normalized pressure versus displacement is ilustrated in Figure (9). The results are in excellent agreement with Prandtl's solution, and both the, regular and Modified Drucker-Prager models present very similar solutions. In this case, the predicted limit pressure is $P_{lim}/c \approx 15$.

Table 1: Material parameters for the soil taken from [6].

Parameter	Value
E(Young's modulus)	$10^7 kPa$
ν(Poisson's ratio)	0.48
c	$490kPa$
ϕ	$20°$

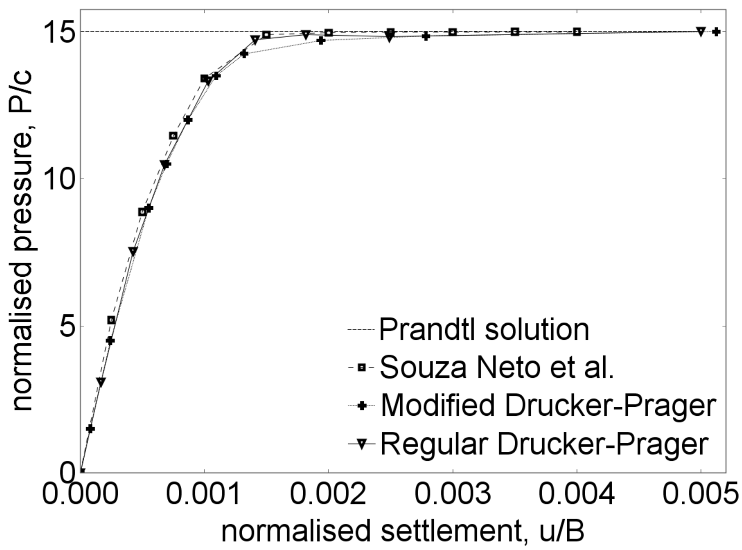

Figure 9: Strip footing. Load-displacement curve, comparing our results with [6].

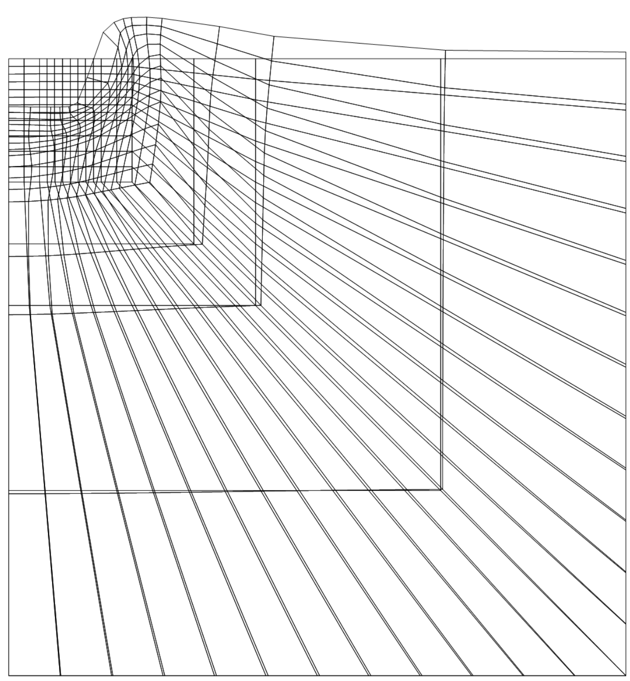

(a)

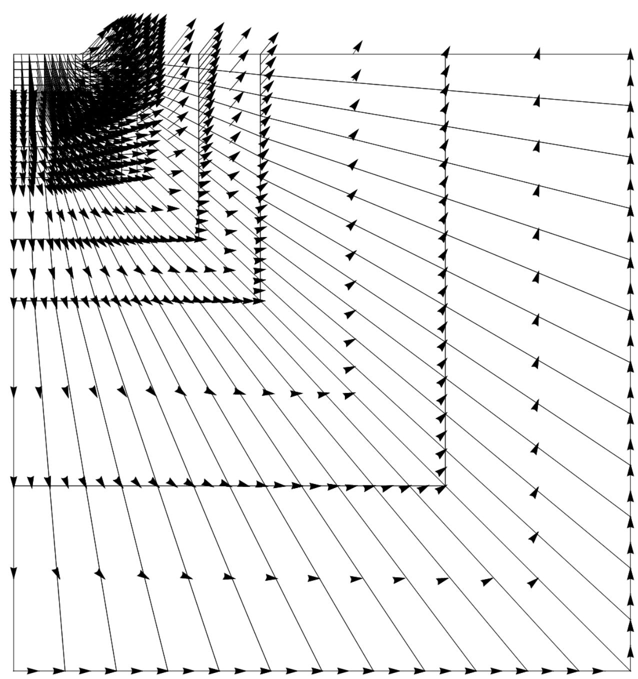

(b)

Figure 10: 9th load step, considering the modified Drucker-Prager. Figure (a) show the deformed mesh and (b) the displacement field. The adopted scale factor is 200.

8.3 Example 3

In this example the plane-strain analysis of an inclined earth embankment subjected to self-weight is performed. The soil is modelled as Modified hyperbolic Druker-Prager material with the material constants shown in Table (2). The material is assumed to be perfectly plastic. The constants A_{md} and B_{md} are defined to be the Drucker–Prager approximation to the Mohr–Coulomb law in plane strain match. The mesh used in the finite

Table 2: Material parameters for the soil taken from [6].

Parameter	Value
E(Young's modulus)	$20000kPa$
ν(Poisson's ratio)	0.49
c	$50kPa$
ϕ	$20°$
γ	$20kN/m^3$

element simulation is illustrated in Figure (11). The mesh is composed of 512 eight-nodes elements. The load was applied in ten steps. Figure (12) show the displacement in point A versus the load factor. The limit analysis of slopes under gravity load is described by [19]. A safety factor based on limit analysis for the present dimensions and material properties predict a maximum load factor of 4.045. For more details about the analytical solution see [6]. The finite element's simulation predicts a failure with a load factor of 4.19, see Figure (12). This represents a 3.4% above the limit analysis solution. Figure (12) compares the solution obtained by [6] using the Mohr-Coulomb model with the present solution considering the hyperbolic Drucker-Prager. Results are very similar.

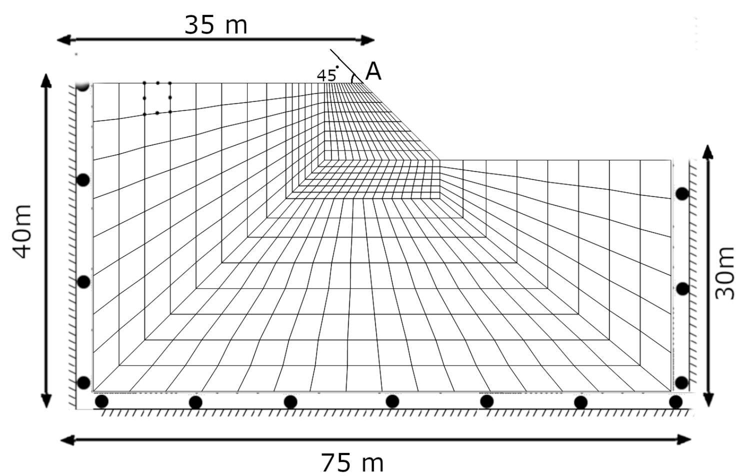

Figure 11: Finite element mesh, geometry and boundary conditions schemes.

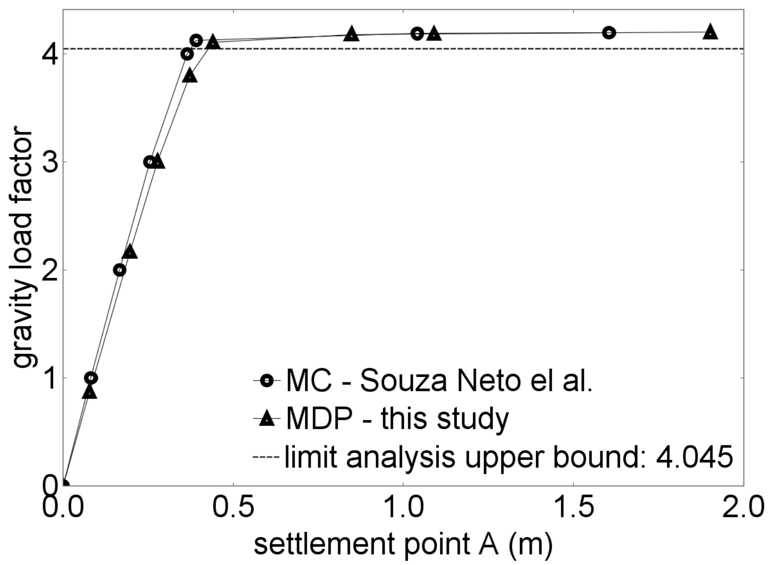

Figure 12: Displacement plotted against the gravity factor. Comparing the present results with [6].

Figure (13) show the incremental plastic multiplier and the displacement field with a gravity load factor of 4.11. The plastic multiplier contours as well as the displacement vector field reproduces the log spiral failure mechanism observed in the collapse of this kind of structure.

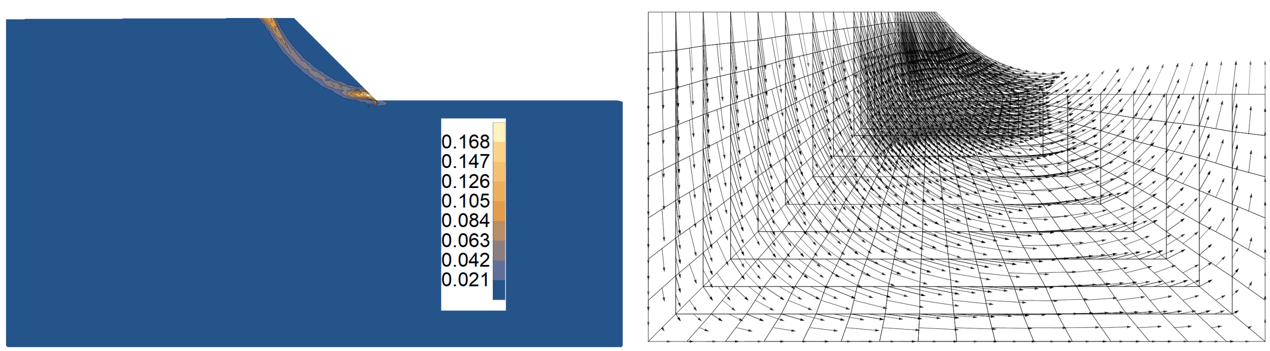

(a) (b)

Figure 13: Figures generated with a gravity load factor of 4.11. (a) Incremental plastic multiplier ($\Delta\gamma$) and (b) displacement vector field with 10 scale factor.

9 Conclusion

A simplified methodology was proposed for elastoplastic calculations, which holds for associative models. It generates a representation of the elastoplastic model based on REMSS and on the fact that, in this coordinate system, the correct return trajectory is the closest-point return. The CPP in REMSS is a powerful approach that allows a straightforward numerical solution of complex computational plasticity models. The rotated space described simplify the constitutive relations and consequently the CPP equations. For perfect plasticity the CPP solution to β is analytical and is the same for Drucker-Prager, von Mises and any other model that has circular shape in the deviatoric section. In this study, the analytical solution for both von Mises and Druker-Prager models were obtained. Also, a numerical solution to a modified hyperbolic Drucker-Prager was presented. The proposed formulation was verified by the application to three finite element examples. The obtained solutions are in excellent agreement with the analytical solutions. The hyperbolic Drucker-Prager produced very similar solution to Mohr-Coulomb in example 3. The models derivatives and the consistent modular matrix are described in the appendix. The code used in this study is available on-line, and can be easily extended to elastoplastic calculations of other models.

References

[1] O. C. Zienkiewicz , S. Valliapan, and I. P. King. Elasto-plastic solutions of engineering problems-The initial stress finite element approach. Int. J. Numer. Methods Eng., 1 (1969), pp. 75-100.

[2] C. G. Nayak and O. C. Zienkiewicz. Elastic-Plastic stress analysis: A generalization for various constitutive relations including strain softening. Int. J. Numer. Methods Eng., 5 (1972), pp. 113-135.

[3] D. R. J. Owen, E. Hinton. Finite Elements in Plasticity. Pineridge Press Limited. (1990).

[4] M. A. Crisfield. Non-Linear Finite Element Analysis of Solids and Structures. Volume 1. John Wiley & Sons Ltd. (1991).

[5] J. C. Simo, T.J.R. Hughes. Computational Inelasticity. Springer. (1997).

[6] E. Souza Neto, D. Peric and D. R. J. Owen. Computational Methods for Plasticity. John Wiley & Sons Ltd. (2008).

[7] M. A. Crisfield. Non-linear Finite Element Analysis of Solids and Structures, Advanced Topics. Volume 2. John Wiley & Sons Ltd. (1997).

[8] J. C. Simo and M. A. Ortiz. A unified approach to finite deformation elastoplastic analysis based on the use of hyperelastic constitutive-equations. Comput. Methods Appl. Mech. Eng. 1985, 492, pp 221-245

[9] F. Armero and A. Pérez-Foguet. On the formulation of closest-point projection algorithms in elastoplasticity—part I: The variational structure. International Journal for Numerical Methods in Engineering, 53 (2) (2002), pp. 297-329. DOI: 10.1002/nme.278

[10] F. Armero and A. Pérez-Foguet. On the formulation of closest-point projection algorithms in elastoplasticity—part II: Globally convergent schemes. International Journal for Numerical Methods in Engineering, 53 (2) (2002), pp. 331-374. DOI: 10.1002/nme.279

[11] Crouch RS, Askes H, Li T. Analytical CPP in energy-mapped stress space: Application to a modified Drucker–Prager yield surface. Comput. Methods Appl. Mech. Engrg. 2009;198:853–859. doi:10.1016/j.cma.2008.10.009

[12] T. J. R. Hughes and K. S. Pister. Consistent linearization in mechanics of solids and structures. Computer & Structures, 8 (1978), pp. 391-397.

[13] R. D. Krieg and D. B. Krieg. Accuracies of numerical solution methods for the elastic-perfectly plastic model. ASME J. Presure Vessel Technol., 1977, 994, 510-515

[14] D.L. Cecílio, P.B.R. Devloo, S.M. Gômes, E.S.R. Santos, N. Shauer. An improved numerical integration algorithm for elastoplastic constitutive equations. Computers and Geotechnics, 64 (2015), pp. 1-9. DOI: 10.1016/j.compgeo.2014.10.013

[15] Coombs WM, Crouch RS. Non-associated reuleaux plasticity: analytical stress integration and consistent tangent for finite deformation mechanics. Comput Methods Appl Mech Eng 2011; 200(9):1021–1037

[16] Borja RI. Plasticity Modeling & Computation. Springer Science & Business Media; 2012.

[17] E. Lainé, C. Vallée and D. Fortuné. Nonlinear isotropic constitutive laws: choice of the three invariants, convex potentials and constitutive inequalities. International Journal of Engineering Science, 37 (15) (1999), pp. 1927-1941. DOI: 10.1016/S0020-7225(99)00006-3

[18] R. Hill. The Mathematical Theory of Plasticity. London: Oxford University Press.(1950).

[19] Chen, Wai-Fah (1975). Limit analysis and soil plasticity. Elsevier, New York.

A Consistent modular matrix

In this section the flow rules $\boldsymbol{\partial\Phi/\partial\sigma}$ and the matrix $\boldsymbol{\partial^2\Phi/\partial\sigma^2}$ are derived for the perfectly plastic and associative von Mises and Drucker-Prager models. They are necessary to compute the consistent modular matrix. Voigt notation is considered, and the full returned stress tensor ($\boldsymbol{\sigma} = [\sigma_{xx}\ \sigma_{yy}\ \sigma_{zz}\ \sigma_{yz}\ \sigma_{xz}\ \sigma_{xy}]$) is obtained making use of Eq. (38).

A.1 von Mises

The yield surface of this model is given by Eq. (39), and the flow rule represented by

$$\boldsymbol{a}(\boldsymbol{\sigma}) = \partial\Phi/\partial\boldsymbol{\sigma} = \frac{\sqrt{3}}{2\sqrt{J_2}}, \boldsymbol{S}. \tag{53}$$

were $\boldsymbol{S} = \boldsymbol{\sigma} - 1/3(\sigma_{xx} + \sigma_{yy} + \sigma_{zz})\ \boldsymbol{I}$. The matrix $(\boldsymbol{\partial a/\partial\sigma})$ is computed in terms of the projected stresses by (54).

$$\frac{\boldsymbol{\partial a}}{\boldsymbol{\partial \sigma}} = \boldsymbol{\partial^2\Phi/\partial\sigma^2} = \frac{\sqrt{3}}{2\sqrt{J_2}}\boldsymbol{P} + \frac{\sqrt{3}}{4J_2^{3/2}}\boldsymbol{S}\otimes\boldsymbol{S}., \tag{54}$$

were $\boldsymbol{P}$ is described in Eq. (64).

A.2 Drucker Prager

The yield surface is given by Eq. (45), and the flow rule is given by

$$\boldsymbol{a}(\boldsymbol{\sigma}) = \frac{A}{3}\boldsymbol{I} + \frac{\sqrt{3}}{2\sqrt{J_2}}\boldsymbol{S}, \tag{55}$$

were $\boldsymbol{I} = [1\ 1\ 1\ 0\ 0\ 0]$. The matrix $\frac{\boldsymbol{\partial a}}{\boldsymbol{\partial\sigma}}$ is given by,

$$\frac{\boldsymbol{\partial a}}{\boldsymbol{\partial \sigma}} = \frac{1}{2\sqrt{J_2}}\boldsymbol{P} - \frac{1}{4J_2^{3/2}}\boldsymbol{S}\otimes\boldsymbol{S}. \tag{56}$$

A.3 Modified Drucker-Prager

$$\boldsymbol{a}(\boldsymbol{\sigma}) = \frac{6\ c\ \cot(\phi) B_{md}^2 \boldsymbol{I} - 2B_{md}^2 I_1 \boldsymbol{I} + 9\ A_{md}^2\ \boldsymbol{S}}{9\ A_{md}^2\ B_{md}^2} \tag{57}$$

$$\frac{\partial \boldsymbol{a}}{\partial \boldsymbol{\sigma}} = \frac{\boldsymbol{P}}{B_{md}^2} - \frac{2\boldsymbol{I} \otimes \boldsymbol{I}}{9\ A_{md}^2} \tag{58}$$

$$A_{md} = \frac{c}{\sqrt{3}\tan(\phi)} - c\cot(\phi),\ B_{md} = A_{md} A \tag{59}$$

A.4 Consitent modular matrix

The incremental plastic multiplier ($\Delta\gamma$) is computed by

$$\Delta\gamma = \frac{||\boldsymbol{\varepsilon}^t - \boldsymbol{\varepsilon}||}{||\boldsymbol{a}||}. \tag{60}$$

To compute $\Delta\gamma$ is necessary the returned stress ($\boldsymbol{\sigma}$) and the flow rule ($\boldsymbol{a}(\boldsymbol{\sigma})$).

The consitent modular matrix $\mathbf{D}^{ep}$ is obtained by enforcing the consistency condition on the discrete algorithmic problem (20). The algorithmic moduli $\boldsymbol{H}$ is defined as

$$\boldsymbol{H} = \left(\boldsymbol{I} + \Delta\gamma \mathbf{D}^e \frac{\partial \boldsymbol{a}}{\partial \boldsymbol{\sigma}}\right)^{-1}\ \mathbf{D}^e, \tag{61}$$

and the consistent modular matrix by,

$$\mathbf{D}^{ep} = \frac{\boldsymbol{H}\ \boldsymbol{a}\ \boldsymbol{a}^T \boldsymbol{H}}{\boldsymbol{a}^T\ \boldsymbol{H}\ \boldsymbol{a}}, \tag{62}$$

were the elastic constitutive matrix is

$$\mathbf{D}^e = \begin{bmatrix} K+4G/3 & K-2G/3 & K-2G/3 & 0 & 0 & 0 \\ K-2G/3 & K+4G/3 & K-2G/3 & 0 & 0 & 0 \\ K-2G/3 & K-2G/3 & K+4G/3 & 0 & 0 & 0 \\ 0 & 0 & 0 & G & 0 & 0 \\ 0 & 0 & 0 & 0 & G & 0 \\ 0 & 0 & 0 & 0 & 0 & G \end{bmatrix}. \tag{63}$$

with $K = \frac{E}{3(1-2\nu)}$ and $G = \frac{E}{2(1+\nu)}$.

$$\boldsymbol{P} = \begin{bmatrix} 2/3 & -1/3 & -1/3 & 0 & 0 & 0 \\ -1/3 & 2/3 & -1/3 & 0 & 0 & 0 \\ -1/3 & -1/3 & 2/3 & 0 & 0 & 0 \\ 0 & 0 & 0 & 2 & 0 & 0 \\ 0 & 0 & 0 & 0 & 2 & 0 \\ 0 & 0 & 0 & 0 & 0 & 2 \end{bmatrix}. \tag{64}$$